Activity-dependent death of transient Cajal-Retzius neurons is required for functional cortical wiring

Martina Riva[1,2,3†], Ioana Genescu[4†], Chloé Habermacher[3,5†], David Orduz[5§], Fanny Ledonne[2], Filippo M Rijli[6], Guillermina López-Bendito[7], Eva Coppola[1,2,3], Sonia Garel[4‡*], Maria Cecilia Angulo[3,5‡*], Alessandra Pierani[1,2,3‡*]

[1]Institut Imagine, Université de Paris, Paris, France; [2]Institut Jacques Monod, CNRS UMR 7592, Université de Paris, Paris, France; [3]Institute of Psychiatry and Neuroscience of Paris (IPNP), INSERM U1266, Université de Paris, Paris, France; [4]Institut de Biologie de l'École Normale Supérieure (IBENS), Département de Biologie, École Normale Supérieure, CNRS, INSERM, Université PSL, Paris, France; [5]INSERM U1128, Paris, France; [6]Friedrich Miescher Institute for Biomedical Research, Basel, Switzerland; [7]Instituto de Neurociencias de Alicante, Universidad Miguel Hernandez, Sant Joan d'Alacant, Spain

*For correspondence:
garel@biologie.ens.fr (SG);
maria-cecilia.angulo@
parisdescartes.fr (MCA);
alessandra.pierani@inserm.fr (AP)

†These authors contributed equally to this work
‡These authors also contributed equally to this work

Present address: §Gfi informatique, Saint-Ouen-sur-Seine, France

Abstract Programmed cell death and early activity contribute to the emergence of functional cortical circuits. While most neuronal populations are scaled-down by death, some subpopulations are entirely eliminated, raising the question of the importance of such demise for cortical wiring. Here, we addressed this issue by focusing on Cajal-Retzius neurons (CRs), key players in cortical development that are eliminated in postnatal mice in part via Bax-dependent apoptosis. Using Bax-conditional mutants and CR hyperpolarization, we show that the survival of electrically active subsets of CRs triggers an increase in both dendrite complexity and spine density of upper layer pyramidal neurons, leading to an excitation/inhibition imbalance. The survival of these CRs is induced by hyperpolarization, highlighting an interplay between early activity and neuronal elimination. Taken together, our study reveals a novel activity-dependent programmed cell death process required for the removal of transient immature neurons and the proper wiring of functional cortical circuits.

Introduction

An emerging player in the assembly of neuronal networks is programmed cell death (PCD). In the nervous system, programmed cell death (PCD) fine-tunes the density of neuronal populations by eliminating 20–40% of overproduced neurons (*Fuchs and Steller, 2011*; *Causeret et al., 2018*; *Wong and Marín, 2019*). Only few populations of the mouse cerebral cortex almost completely disappear during the first two postnatal weeks. Amongst these, Cajal-Retzius cells (CRs), the first-born cortical neurons lying in the superficial Layer I (LI), undergo extensive cell death in the mouse during the second postnatal week (*Ledonne et al., 2016*). The persistence of CRs during postnatal life is increased in malformations of cortical development (MCDs) and epilepsies thereby opening the intriguing possibility that the maintenance of CRs contributes to the dysfunction of cortical circuits (for review see *Luhmann, 2013*).

CR play pivotal roles at multiple steps of early cortical development, in addition to their best-known role in the control of radial migration (*Ishii et al., 2016*). They comprise three molecularly distinct subtypes which migrate from different sources that surround the cortical primordium: (i) septum

and eminentia thalami-derived CRs of the ΔNp73/Dbx1 lineage (SE-CRs); (ii) hem-derived CRs of the ΔNp73/Wnt3a lineage (hem-CRs); (iii) pallial-subpallial boundary-derived CRs of the Dbx1 lineage (PSB-CRs) (*Bielle et al., 2005*; *Yoshida et al., 2006*; *Tissir et al., 2009*). Our previous work revealed that their specific embryonic distribution in distinct territories plays key functions in wiring of cortical circuits by controlling the size of functional areas, both primary and higher-order, as well as targeting of thalamocortical afferents (*Griveau et al., 2010*; *Barber et al., 2015*; *Barber and Pierani, 2016*). More recently, we showed that subtype-specific differences also exist in their elimination during early postnatal life, with SE- but not hem-derived CRs dying in a Bax-dependent manner, which is a critical player of the apoptotic pathway (*Ledonne et al., 2016*).

Before their disappearance, CRs express ionotropic glutamatergic and GABAergic receptors and are embedded into immature circuits where they mainly receive GABAergic synaptic inputs, suggesting that these transient cells might have an activity-dependent role in the development of cortical networks (*Kirischuk et al., 2014*). Consistently, we found that CRs density shapes axonal and dendritic outgrowth in LI and impacts onto the excitation/inhibition (E/I) ratio in upper cortical layers (*de Frutos et al., 2016*). Conversely, activity was also proposed as one of the drive of CR demise. Studies from *Del Río et al. (1996)* first highlighted the role played by electrical activity on CR death in vitro. CRs were shown to display electrophysiological features of immature neurons (*Kirischuk et al., 2014*; *Barber and Pierani, 2016*), including the persistent depolarizing action of GABA which was suggested to depend on the maintenance of the chloride inward transporter NKCC1 and the absence of the outward transporter KCC2 (*Mienville, 1998*; *Achilles et al., 2007*; *Pozas et al., 2008*). Interestingly, pharmacological inhibition of activity and GABA signaling in vitro and global inactivation of NKCC1 in vivo were shown to reduce the death of CRs (*Blanquie et al., 2017a*; *Blanquie et al., 2017b*). However, very little is known on the role of electrical activity in CR subtype-specific death in vivo, as well as its contribution to the construction of functional and dysfunctional cortical circuits.

Here we show that hyperpolarization of CR neurons by Kir2.1-dependent expression prevented cell death of ΔNp73- but not Wnt3a-derived CRs, corresponding to SE-CRs. By comparing two different mutants in which CR death was similarly rescued, we found that abnormal SE-CR survival promotes exuberance of dendrites and spine density in pyramidal neurons in an activity-dependent manner. This results in an E/I imbalance due to an increase in the excitatory drive of upper cortical neurons. Our findings show that neuronal activity is involved in CR subtype-specific death and argue in favor of an unappreciated role of the disappearance of these transient neurons in controlling the morphology of pyramidal neurons and the functional properties of their cortical excitatory networks at postnatal stages.

Results

Subsets of CRs die in an activity-dependent manner

The ΔNp73$^{cre/+}$ mouse line targets approximately 80% of CRs, namely hem-CRs (Wnt3a lineage) and SE-CRs (*Tissir et al., 2009*; *Griveau et al., 2010*; *Yoshida et al., 2006*). ΔNp73-CRs, but not Wnt3a-derived hem-CRs, were shown to be eliminated postnatally via Bax-dependent death, indicating that SE-CRs undergo apoptosis. However, the trigger of such apoptosis or the mechanisms regulating the death of other CR populations are still unknown (*Ledonne et al., 2016*). To decipher whether activity might regulate the death of specific subsets of CRs in vivo, we first overexpressed the hyperpolarizing channel Kir2.1 (R26$^{Kir2.1mcherry/+}$) (*Moreno-Juan et al., 2017*) using the ΔNp73$^{cre/+}$ line. Tracing of CRs at several postnatal stages in control and Kir2.1-expressing mice was performed using DsRed immunostainings to visualize tdTomato and mcherry reporters, respectively. We found that the density of CRs in the somatosensory barrel cortex was unchanged in these animals at postnatal day 7 (P7), that is before CRs undergo massive cell death (*Figure 1A and B*). In contrast, Kir2.1 channel overexpression in ΔNp73-CRs resulted in an increase of CRs with respect to controls in the somatosensory cortex at P15 and P25 (*Figure 1A and B*). Importantly, using whole-cell recording, we checked that rescued CRs were, as expected, hyperpolarized and displayed a decrease in the input resistance without exhibiting changes in action potential properties at both P15 and P25 (*Figure 1—figure supplement 1A-C*). Biocytin-filling and immunostaining further revealed that most morphological properties were preserved in Kir2.1-expressing CRs, apart from a reduced soma at
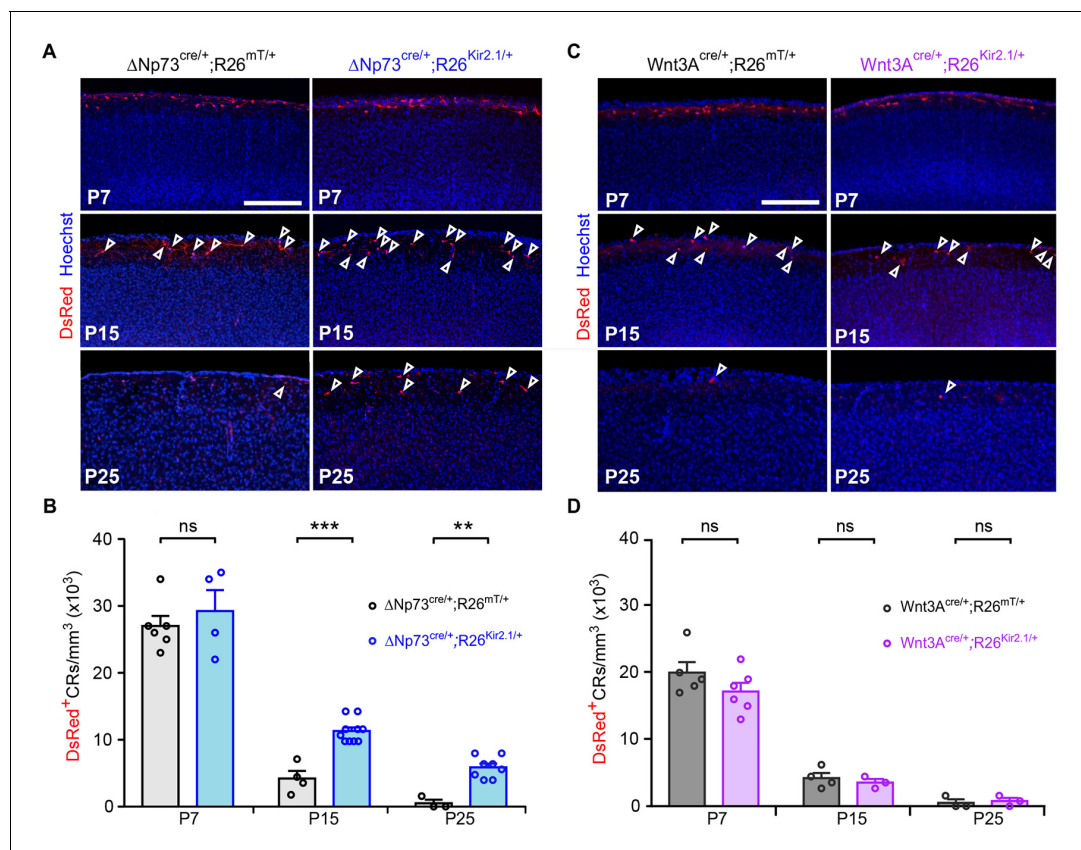
Figure 1. Hyperpolarization induces the survival of SE-CRs. (**A**) Confocal images of cortical sections from P7, P15 and P25 $\Delta Np73^{cre/+};R26^{mT/+}$ controls (left) and $\Delta Np73^{cre/+};R26^{Kir2.1/+}$ mutants (right) stained for DsRed (red) and Hoechst (blue). Arrowheads indicate DsRed⁺ CRs at P15 and P25. (**B**) Quantification of CR density (CRs/mm³) at the pial surface in the somatosensory (S1) cortex (P7: n = 6 for controls and n = 4 for mutants, p=0.716; P15: n = 4 for controls and n = 10 for mutants, p=0.001; P25: n = 3 for controls and n = 8 for mutants, p=0.006). (**C**) Confocal images of cortical sections from P7, P15 and P25 Wnt3a$^{cre/+};R26^{mT/+}$ controls (left) and Wnt3a$^{cre/+};R26^{Kir2.1/+}$ mutants (right) stained for DsRed (red) and Hoechst (blue). Arrowheads indicate DsRed⁺ CRs at P15 and P25. For simplicity, arrowheads were not displayed at P7, as there are too many CRs at this stage. (**D**) Quantification of CR density (CRs/mm³) at the pial surface in the somatosensory (S1) cortex (P7: n = 5 for controls and n = 6 for mutants, p=0.2251; P15: n = 4 for controls and n = 3 for mutants, p=0.771; P25: n = 3 for controls and n = 3 for mutants, p=0.813). Mann-Whitney U Test. Scale bar represents 200 µm. Data used for quantitative analyses as well as the numerical data that are represented in graphs are available in *Figure 1—figure supplement 1—source data 1*. The online version of this article includes the following source data and figure supplement(s) for figure 1:

Figure supplement 1. Electrophysiological properties and morphology of rescued CRs in $\Delta Np73^{cre/+}; R26^{Kir2.1/+}$ mice.
Figure supplement 1—source data 1. Density and properties of CRs in the Kir2.1 model.

P25 (*Figure 1—figure supplement 1D*). In particular, rescued CRs displayed similar branching length in LI (*Figure 1—figure supplement 1B and E*) and co-expressed Reelin (Reln) from P7 to P25 (*Figure 1—figure supplement 1F and G*). Taken together, these experiments show that hyperpolarization of $\Delta Np73$-CRs does not drastically alter cardinal morphological features of CRs but prevents their complete elimination.

A similar proportion of CRs were rescued either by hyperpolarization (*Figure 1A and B*) or by preventing apoptosis (*Ledonne et al., 2016*), raising the intriguing possibility that the same subpopulation of CRs, SE-CRs, might be preserved in both conditions. Since hem-CRs are not eliminated via a Bax-dependent process (*Ledonne et al., 2016*), we investigated whether their survival is sensitive to hyperpolarization. We thus overexpressed Kir2.1 specifically in hem-CRs using the Wnt3a$^{cre/+}$, which corresponds to about 70% of the $\Delta Np73$-CRs at early postnatal stages (*Figure 1C and D*). We found that hem-CR death was unaffected in this mouse line (*Figure 1C and D*). Moreover, taking into account cortical growth, the proportions of rescued cells in the somatosensory cortex at P25 was evaluated to approximately 30% of the initial pool of $\Delta Np73$-CRs, which corresponds to the expected number of SE-CRs (*Bielle et al., 2005*; *Yoshida et al., 2006*; *Tissir et al., 2009*).

Collectively, these results show that the death of a specific subset of $\Delta Np73^{cre/+}$ SE-CRs is both Bax-dependent and activity-dependent.

CRs rescued by hyperpolarization or blocking Bax-dependent apoptosis are integrated in neuronal circuits

It has been established that CRs are integrated in functional circuits early in the developing postnatal neocortex (*Kilb and Luhmann, 2001*; *Soda et al., 2003*; *Sava et al., 2010*; *Cocas et al., 2016*). CRs receive GABAergic synaptic inputs and, despite the expression of NMDA receptors (NMDARs) on CR membranes, the presence of NMDAR-mediated synaptic responses is still under debate (*Kilb and Luhmann, 2001*; *Soda et al., 2003*; *Sava et al., 2010*; *Schwartz et al., 1998*; *Mienville and Pesold, 1999*; *Radnikow et al., 2002*; *Anstötz et al., 2014*). To test whether CRs harbored functional GABAergic and/or glutamatergic synapses during the cell death period and after their rescue, we recorded spontaneous (sPSCs) and evoked postsynaptic currents (ePSCs) of fluorescent CRs with a KCl-based intracellular solution. First, at P9-11 in control $\Delta Np73^{cre/+}$;$R26^{mt/+}$ mice, sPSCs sensitive to the $GABA_A$ receptor ($GABA_A$R) antagonist SR95531 (10 µM) were observed in CRs held at −60 mV, confirming that CRs are innervated mainly by functional GABAergic synaptic inputs (*Figure 2—figure supplement 1A–B*; data not shown for SR95531 application; n = 7). Low-frequency stimulations in LI easily elicited ePSCs that were also completely blocked by SR95531 application (*Figure 2—figure supplement 1C–D*), even in 0 mM Mg^{2+} condition, which relieves the Mg^{2+} block of NMDA receptors. Taken together, these results indicate that ePSCs were mediated by $GABA_A$Rs and not by AMPA or NMDA receptors. In agreement with previous studies (*Sun et al., 2019*), the presence of GABAergic synaptic inputs on CRs was confirmed by immunostainings against the presynaptic marker GAD65/67 and the postsynaptic marker Gephyrin (*Figure 2—figure supplement 1E*). Since the depolarizing action of GABA in CRs was proposed to be partly due to the lack of expression of KCC2, the chloride transporter responsible for maintaining a low intracellular chloride concentration (*Mienville, 1998*; *Achilles et al., 2007*; *Pozas et al., 2008*; *Blanquie et al., 2017a*; *Blanquie et al., 2017b*), we also checked for the protein expression of this transporter. In agreement with previous reports (*Achilles et al., 2007*; *Pozas et al., 2008*), control GFP^+ CRs in $\Delta Np73^{cre/+}$;$Tau^{GFP/+}$ mice expressed very low to undetectable levels of KCC2 (*Figure 2—figure supplement 1F*). Thus, during the timeperiod of their activity-dependent death, CR cells receive solely GABAergic synaptic inputs.

We further explored whether these inputs are maintained at later stages, when CR cells are not eliminated. To this aim, we performed the same experiments at P23-28 in $\Delta Np73^{cre/+}$;$R26^{Kir2.1/+}$ and $\Delta Np73^{cre/+}$;$Bax^{lox/lox}$;$R26^{mT/+}$ mice (*Figure 2A–B*). First, we found that sPSCs in rescued CRs had similar frequencies, amplitudes and kinetics in both models (*Figure 2A–B*). Moreover, sPSCs were completely abolished by $GABA_A$R antagonist SR95531, indicating that rescued CRs remained innervated by functional GABAergic synaptic inputs (data not shown for SR95531 application, n = 8 and n = 5 for $\Delta Np73^{cre/+}$;$R26^{Kir2.1/+}$ and $\Delta Np73^{cre/+}$;$Bax^{lox/lox}$;$R26^{mT/+}$ mice, respectively). Consistently, the complete block of ePSCs by SR95531, even in 0 mM Mg^{2+}, revealed that ePSCs were exclusively mediated by $GABA_A$Rs at hyperpolarized holding potentials, as observed in younger mice (*Figure 2C–D* and *Figure 2—figure supplement 1C–D*). While these GABAergic inputs were preserved in rescued CRs, we observed a reduced sPSC frequency and ePSC amplitude compared to P9-P11 mice, suggesting a decreased CR connectivity in the more mature neocortex (*Figure 2A–B* and *Figure 2—figure supplement 1A–B*).

Altogether, these results indicate that rescued CRs, as previously showed in the early postnatal neocortex (*Soda et al., 2003*; *Sava et al., 2010*; *Kilb and Luhmann, 2001*), receive solely GABAergic synaptic inputs at the time of their death. They further demonstrate that rescued CRs in both mouse models, inspite of a reduced connectivity compared to earlier stages, are kept integrated in functional neuronal circuits.

Survival of electrically-active CRs triggers dendritic exuberance of upper layer pyramidal neurons

In order to test whether CR aberrant survival may alter the function of other neurons in upper cortical layers, we used biocytin-filling and confocal 3D reconstructions to study the morphology of Layer II (LII) and LIII pyramidal neurons in the somatosensory barrel cortex of both $\Delta Np73^{cre/+}$;$R26^{Kir2.1/+}$
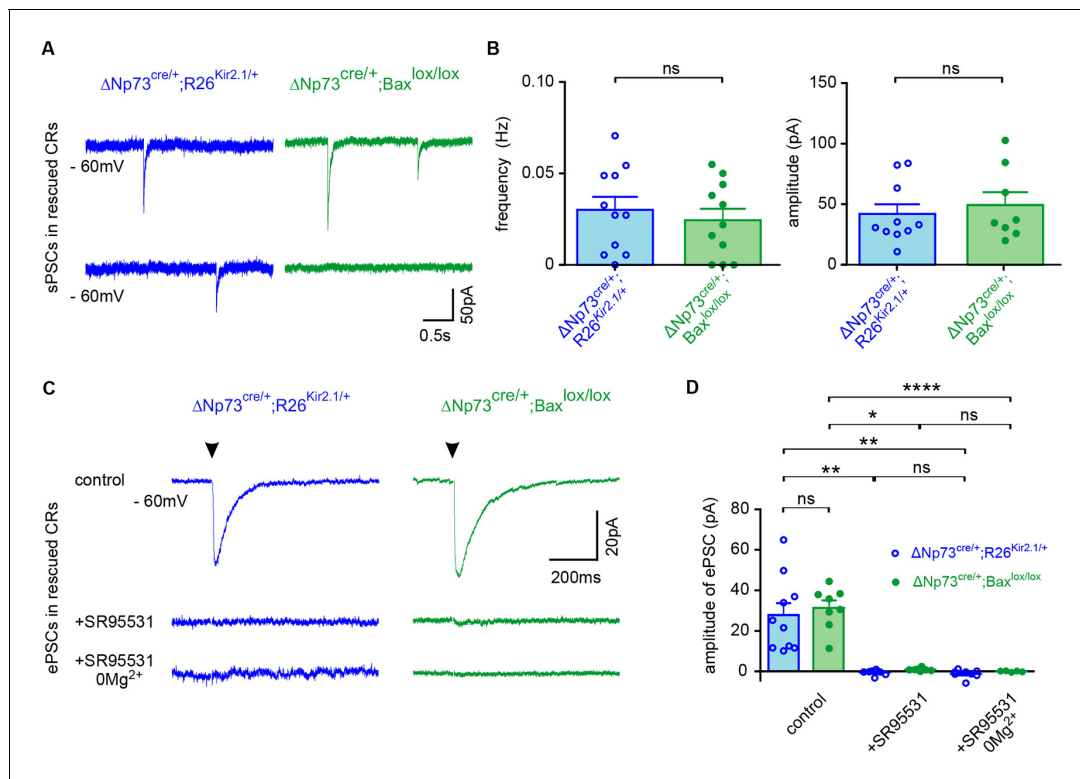
Figure 2. Pure GABAergic sPSCs and ePSCs in rescued CRs. (**A**) Spontaneous PSCs (sPSCs) recorded in rescued CRs from $\Delta Np73^{cre/+}$;$R26^{Kir2.1/+}$ at P27 (blue) and $\Delta Np73^{cre/+}$;$Bax^{lox/lox}$ mutants at P26 (green), respectively. (**B**) Plots of the frequency and amplitude of sPSCs (n = 11 for $\Delta Np73^{cre/+}$; $R26^{Kir2.1/+}$ and n = 11 for $\Delta Np73^{cre/+}$; $Bax^{lox/lox}$ mice at P24-29; frequency: p=0.552, amplitude: p=0.580, Student T Test). Rise time is 2.10 ± 0.42 ms vs 1.02 ± 0.20 ms and decay time 34.26 ± 6.39 ms vs 29.14 ± 3.56 ms for $\Delta Np73^{cre/+}$;$R26^{Kir2.1/+}$ and $\Delta Np73^{cre/+}$;$Bax^{lox/lox}$ mice, respectively. (**C**) Mean evoked PSCs (ePSCs) for rescued CRs respectively from a $\Delta Np73^{cre/+}$;$R26^{Kir2.1/+}$ mutant at P29 (blue) and a $\Delta Np73^{cre/+}$;$Bax^{lox/lox}$ mutant at P26 (green) upon stimulation of LI neuronal fibers (stimulation time, arrowhead) in control conditions (top), with SR95531 (middle) and SR95531 in Mg^{2+}-free solution (bottom). Note that ePSCs completely disappeared after bath application of SR95531. (**D**) Amplitudes of ePSCs in control conditions, with SR95531 and with SR95531 in Mg^{2+}-free solution ($\Delta Np73^{cre/+}$;$R26^{Kir2.1/+}$ mice at P24-29: $n_{control} = 10$, $n_{SR95531} = 8$ and $n_{SR95531}/Mg2+free$=8; $\Delta Np73^{cre/+}$;$Bax^{lox/lox}$: $n_{control} = 8$, $n_{SR95531} = 5$ and $n_{SR95531}/Mg2+free$=5; Kruskal-Wallis test followed by a Bonferroni multiple comparison when comparing the three conditions for each mutant; Student T test for comparison of control ePSCs between $\Delta Np73^{cre/+}$;$R26^{Kir2.1/+}$ and $\Delta Np73^{cre/+}$;$Bax^{lox/lox}$ mutants, p=0.638). To detect CRs in $\Delta Np73^{cre/+}$;$Bax^{lox/lox}$ mutants the $R26^{mT/+}$ reporter line was used. Data used for quantitative analyses as well as the numerical data that are represented in graphs are available in *Figure 2—figure supplement 1—source data 1*.

The online version of this article includes the following source data and figure supplement(s) for figure 2:

Figure supplement 1. Pure GABAergic sPSCs and ePSCs in control CRs during early postnatal development.

Figure supplement 1—source data 1. Evoked and Spontaneous PSCs in rescued and developing CRs.

and $\Delta Np73^{cre/+}$;$Bax^{lox/lox}$ mice. While no major changes were observed in the morphology of LII/III pyramidal neurons of $\Delta Np73^{cre/+}$;$R26^{Kir2.1/+}$ mice compared to their matched controls (*Figure 3—figure supplement 1*), major defects were observed for these neurons in $\Delta Np73^{cre/+}$;$Bax^{lox/lox}$ mutants (*Figure 3*). Quantitative analyses revealed an increase in the number of apical and basal dendritic branches at P25 in $\Delta Np73^{cre/+}$;$Bax^{lox/lox}$ compared to controls (*Figure 3B*). In order to further characterize cell complexity in relation with the distance from the soma, we performed a Sholl analysis. We observed that LII/III pyramidal cells displayed an increased complexity for apical dendrites (between 180 µm and 240 µm from the soma) as well as for basal dendrites (between 60 and 80 µm from the soma) (*Figure 3C*). Interestingly, no statistically different changes in the number of dendritic branches (*Figure 3—figure supplement 1B*) or the complexity of apical and basal dendrites (*Figure 3—figure supplement 1C*) were detected in LII/LIII pyramidal neurons of the $\Delta Np73^{cre/+}$;$R26^{Kir2.1/+}$ model, in which SE-CRs survive but are hyperpolarized. Thus, the survival of a specific subset of CRs has a general promoting impact onto the dendritic tree of upper layer pyramidal neurons only when they keep their normal intrinsic excitability. Collectively, our analyses show
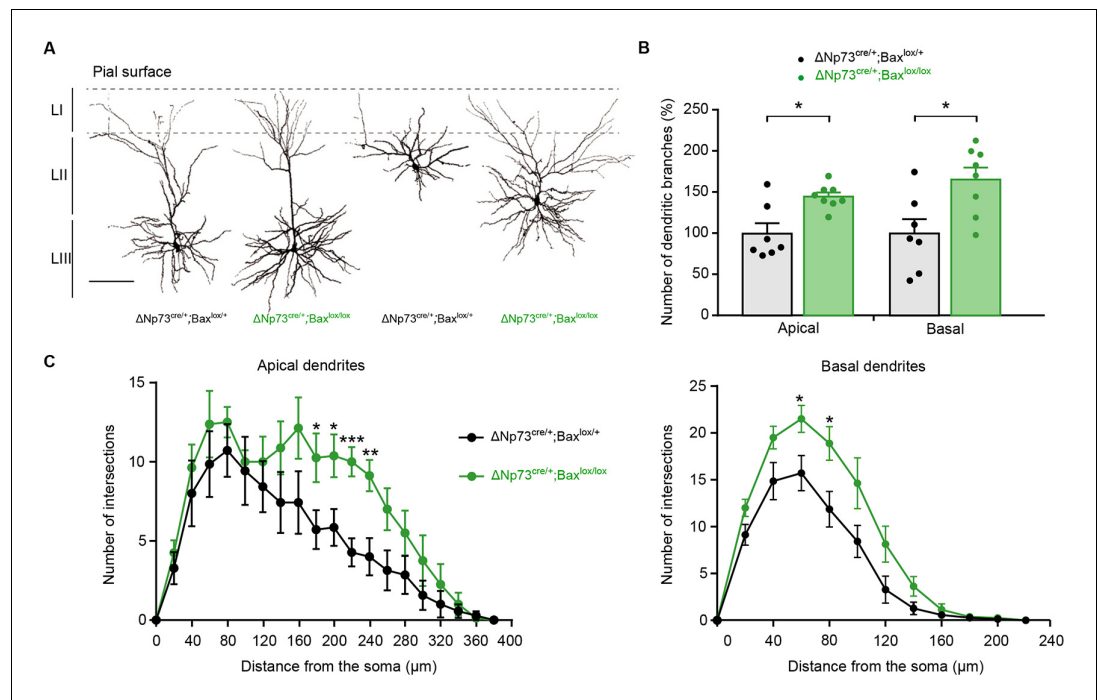
Figure 3. Increased dendritic branches in LII/LIII pyramidal neurons of $\Delta Np73^{cre/+};Bax^{lox/lox}$ mutants. (**A**) Representative examples of LII/III pyramidal neurons filled with biocytin in control (P25) and $\Delta Np73^{cre/+};Bax^{lox/lox}$ mutant (P24) somatosensory cortex. (**B**) Quantification of the number of dentritic branches in control and $\Delta Np73^{cre/+};Bax^{lox/lox}$ mutant LII/III pyramidal neurons, expressed as a percentage of dendritic branches relative to the mean of controls (n = 7 for controls and n = 8 for mutants at P23-28 p=0.0182 for apical dendrites and p=0.014 for basal dendrites; Mann-Whitney U Test). (**C**) Sholl analysis for the apical and basal dendrites in control and $\Delta Np73^{cre/+};Bax^{lox/lox}$ mutants showing an increased cell complexity between 180 and 240 µm (p-value=0.04, 0.027, 0.0007 and 0.005, respectively) and 60 and 80 µm (p value=0.027 and 0.019, respectively) from the soma, respectively (n = 7 for controls and n = 8 for mutants). Multiple T-test. Scale bar represents 100 µm. Data used for quantitative analyses as well as the numerical data that are represented in graphs are available in *Figure 3— figure supplement 1—source data 1*.

The online version of this article includes the following source data and figure supplement(s) for figure 3:

Figure supplement 1. Morphological reconstruction of LII/III pyramidal neurons *in* $\Delta Np73^{cre/+};R26^{Kir2.1/+}$ mutants.
Figure supplement 1—source data 1. Morphological analyses of layer II/III pyramidal cells in the Bax and Kir2.1 models.

that SE-CRs survival in LI promotes an exuberance of apical and basal dendrites of LII/LIII pyramidal neurons in an activity-dependent manner.

Survival of electrically-active CRs increases excitatory entries in upper layer pyramidal neurons

To examine whether the defects of the dendritic arborization of LII/III pyramidal neurons were related to changes in the synaptic inputs received by these neurons, we first examined spines on both apical and basal dendrites of biocytin-filled pyramidal cells (*Figure 4A–D*). Because excitatory synapses are formed on dendritic spines, the latter can be used as a proxy for the quantification of those synapses. For apical dendrites, we examined terminal ramifications in LI, whereas for basal dendrites, we considered horizontal branches approximately at the same distance from the soma. Spine density on both apical and basal dendrites of pyramidal cells was significantly increased in $\Delta Np73^{cre/+};Bax^{lox/lox}$ mutants compared to controls (*Figure 4A and B*) whereas no differences were observed in $\Delta Np73^{cre/+};R26^{Kir2.1/+}$ mutants (*Figure 4C and D*). These results indicate that the survival of electrically-active CRs not only triggers a dendritic exuberance, but also drives an increase in spine densities.
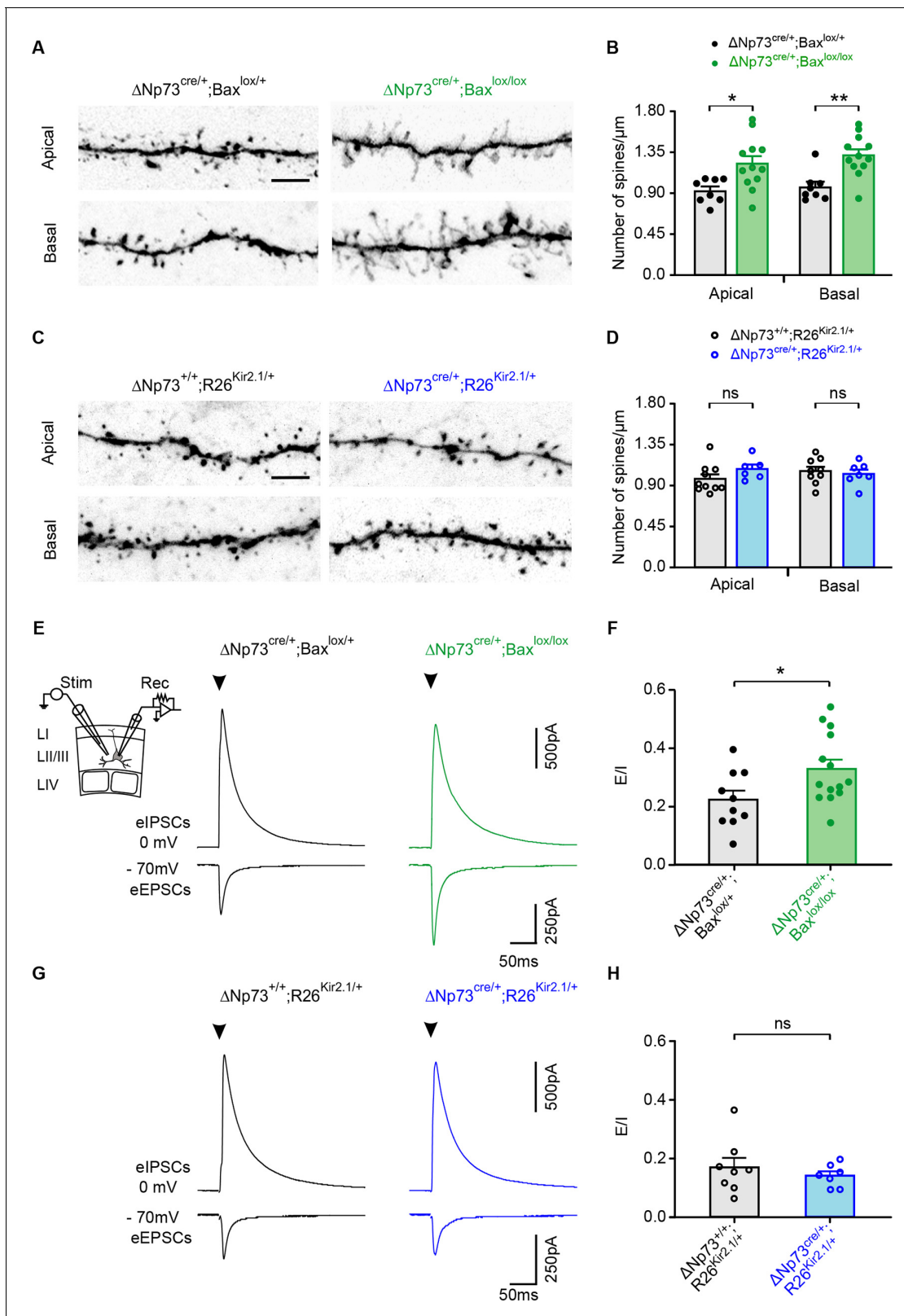
Figure 4. Spine density and evoked synaptic activity recorded in LII/LIII pyramidal neurons in both ΔNp73$^{cre/+}$;Bax$^{lox/lox}$ and ΔNp73$^{cre/+}$;R26$^{Kir2.1/+}$ mutants. (**A, C**) Representative confocal images showing spines in apical and basal dendritic segments of controls (left) and ΔNp73$^{cre/+}$;Bax$^{lox/lox}$ (**A**, right) and ΔNp73$^{cre/+}$;R26$^{Kir2.1/+}$ mutants (**C**, right) at P24-25. (**B, D**) Quantification of the spine density (number of spines/μm) in apical and basal dendrites in LII/LIII pyramidal neurons for both controls and mutants from the same litters (for ΔNp73$^{cre/+}$;Bax$^{lox/lox}$ apical and basal dendrites: n = 8 for

Figure 4 continued on next page

Figure 4 continued

controls and n = 12 for mutants at P23-28, p=0.012 for apical dendrites and p=0.0014 for basal dendrites; for ΔNp73$^{cre/+}$;R26$^{Kir2.1/+}$ apical dendrites: n = 10 for controls and n = 6 for mutants at P23-P29, p=0.166; basal dendrites: n = 9 for controls and n = 7 for mutants, p=0.652; Mann-Whitney U Test). Scale bar represents 5 μm. (E, G) Pyramidal neurons recorded in voltage-clamp at −70 mV and 0 mV in control at P26 (E, left) and P24 (G, left) and in a ΔNp73$^{cre/+}$;Bax$^{lox/lox}$ mutant at P23 (E, right) and a ΔNp73$^{cre/+}$;R26$^{Kir2.1/+}$ mutant at P28 (G, right) during the extracellular stimulation of LII/III fibers as indicated (E, inset). Stimulation artefacts were blanked for visibility. The stimulation time is indicated (arrowheads). (F, H) Plots of E/I ratio calculated from eEPSCs and eIPSCs in controls and ΔNp73$^{cre/+}$;Bax$^{lox/lox}$ mutants (F) and ΔNp73$^{cre/+}$; R26$^{Kir2.1/+}$ mutants (H) (for ΔNp73$^{cre/+}$;Bax$^{lox/lox}$: n = 10 for controls and n = 14 for mutants, p=0.031, Student T Test; for ΔNp73$^{cre/+}$;R26$^{Kir2.1/+}$: n = 8 for controls and n = 7 for mutants, p=0.612; Mann-Whitney U Test). Data used for quantitative analyses as well as the numerical data that are represented in graphs are available in *Figure 4—figure supplement 1—source data 1*.

The online version of this article includes the following source data and figure supplement(s) for figure 4:

Figure supplement 1. Evoked and spontaneous EPSCs and IPSCs of LII/LIII pyramidal neurons in ΔNp73$^{cre/+}$;Bax$^{lox/lox}$ and ΔNp73$^{cre/+}$;R26$^{Kir2.1/+}$ mutants.

Figure supplement 1—source data 1. Spine densities, evoked and spontaneous PSCs in LII/III pyramidal neurons in both Bax and Kir2.1 models.

To test whether these morphological modifications in ΔNp73$^{cre/+}$;Bax$^{lox/lox}$ mutants is accompanied by modifications in excitatory synaptic inputs, we performed whole-cell recordings of upper layer pyramidal neurons during the extracellular stimulation of LII/III fibers. First, the membrane potential of recorded cells was maintained at −70 mV or 0 mV to respectively record evoked excitatory (eEPSCs) and inhibitory (eIPSCs) postsynaptic currents. Pyramidal cells in ΔNp73$^{cre/+}$;Bax$^{lox/lox}$ mutants showed a significant increase in the mean amplitude of eEPSCs, while that of eIPSCs remained unchanged compared to controls (*Figure 4E*, *Figure 4—figure supplement 1A*). This modification is highlighted by a significant increase in the E/I ratio (*Figure 4F*). Together with the increased spine density, these data strongly suggest that pyramidal neurons have enhanced excitatory synaptic inputs. To corroborate this possibility, we then analyzed the spontaneous EPSCs (sEPSCs) of recorded pyramidal neurons. As expected for an increased number of inputs, the sEPSC frequency was significantly higher in ΔNp73$^{cre/+}$;Bax$^{lox/lox}$ mutants with respect to controls while the mean sEPSC amplitude remained unchanged (*Figure 4—figure supplement 1C-D*). When the same experiments were performed in ΔNp73$^{cre/+}$;R26$^{Kir2.1/+}$ mutants, no differences were observed either in the amplitudes of both eEPSCs and eIPSCs or in the E/I ratio (*Figure 4G–H*, *Figure 4—figure supplement 1B*). In line with this, changes were neither observed in the frequency of sEPSCs of these mutants (*Figure 4—figure supplement 1E*), showing that defects in the synaptic activity of pyramidal neurons is dependent on the intrinsic activity of rescued CRs. To test whether the effect on pyramidal cells could be due to a direct action of CR activity on excitatory circuits, we produced ΔNp73$^{cre/+}$;Bax$^{lox/lox}$; ChR2$^{lox/+}$ mutant mice to photoactivate rescued CRs while recording neuronal network activity. After defining an efficient photostimulation protocol for reliably eliciting action potentials on recorded CRs (*Figure 4—figure supplement 1F*), we combined photostimulation with of Layer I interneuron recordings in whole-cell configuration and/or local field potentials (LFPs) in different layers (*Figure 4—figure supplement 1G*). We could never detect light-evoked responses during patch-clamp or extracellular recordings, even in the presence of 0 mM Mg^{2+}, 3 mM Ca^{2+} and 50 μM of the potassium channel blocker 4AP, a treatment that renders all neurons more excitable (*Figure 4—figure supplement 1G*). Although these results do not rule out that rescued CRs contact other neurons through *bona fide* glutamatergic synapses, the low proportion of these cells compared to pyramidal neurons and the lack of electrical extracellular responses during their sustained light stimulation suggest that direct synaptic inputs from CRs cannot account for the robust morphological and functional changes induced in pyramidal cells by the aberrant CR survival.

Overall, these experiments show that the survival of electrically-active SE-CRs increases the excitatory inputs to upper pyramidal neurons, possibly through a non-glutamatergic mechanism, thereby generating a E/I imbalance and functional changes in circuit wiring.

Discussion

Our results show that the elimination of specific subsets of CRs, SE-CRs, is activity-dependent and that this process is essential for proper cortical wiring. Indeed, the persistence of SE-CRs beyond their normal phase of elimination triggered major deficits in LII/LIII somatosensory pyramidal

neurons. Not only the analyzed neurons displayed an increased dendritic arborization and spine density, but they also consistently showed enhanced excitatory inputs leading to a functional E/I imbalance. Remarkably, these anatomical and electrophysiological deficits all relied on the fact that persistent CRs were electrically-active. Our study thus demonstrates that activity is required to eliminate SE-CRs, whose survival would otherwise perturb cortical wiring in an activity-dependent manner. Taken together, it reveals an elegant interplay between transient CRs and neuronal activity in the construction of functional cortical excitatory circuits.

CR subtype-specific pathways in programmed cell death

Activity was reported to promote survival of both glutamatergic and GABAergic neurons in the neocortex and in general in the nervous system (*Blanquie et al., 2017a*; *Causeret et al., 2018*; *Wong and Marín, 2019*), providing a mean to integrate around 70% of neurons into functional circuits. CRs, which completely undergo programmed cell death in the cerebral cortex (*Ledonne et al., 2016*; *Causeret et al., 2018*), have been previously proposed to behave differently. These neurons display 'immature' features such as a depolarized resting potential and a very high input resistance (*Kirischuk et al., 2014*). Especially, GABA is depolarizing in these cells due to their elevated intracellular chloride concentration resulting from the activity of the chloride inward transporter NKCC1 in the absence of expression of chloride outward transporter KCC2 (*Mienville, 1998*; *Achilles et al., 2007*; *Pozas et al., 2008*). Interestingly, the pharmacological blockade of NKCC1 in cell cultures or the genetic ablation of this transporter in vivo promotes the survival of a CR population, probably by preventing $GABA_A$ receptor-mediated depolarization (*Blanquie et al., 2017b*). It must be considered, however, that the depolarizing effect of GABA will depend most probably on the levels of neuronal activity since high activity levels attenuate the $GABA_A$ receptor-mediated excitatory drive in CRs (*Kolbaev et al., 2011*). Here, we confirmed that CRs receive exclusively functional GABAergic synaptic inputs and express low levels of KCC2 in the second postnatal week, that is during the period of massive cell death. Our findings raise the question of the identity of possible GABAergic neurons that regulate CR subtype elimination. CRs receive GABAergic synaptic inputs from different sources, including local interneurons of Layer I, the underlying layers of the neocortex and the subplate, a transient cortical structure absent in the fourth postnatal week, as well as the zona incerta (*Kirmse et al., 2007*; *Myakhar et al., 2011*; *Kirischuk et al., 2014*; *Chen and Kriegstein, 2015*; *Sun et al., 2019*). A related issue is how GABAergic inputs to CRs might change overtime, since we found that rescued CRs receive less inputs than at earlier stages. One interesting possibility is that rescued CRs in Layer I might lose GABAergic innervation from transient or distant populations (i.e. subplate and zona incerta) during maturation of neuronal networks, restricting their connectivity with more local neocortical inputs. Further investigation is needed to determine the different interneuron subtypes impinging on CRs in immature cortical circuits and after their aberrant survival in adults.

Using conditional Kir2.1 expression in a large subpopulation of CRs, we unequivocally show that only a specific subset of CRs, SE-CRs, dies in an activity-dependent manner in vivo. Since CRs are highly hyperpolarized in this mouse model, a plausible explanation is that GABAergic inputs cannot exert their depolarizing effect as in normal conditions, thereby preventing cell death. In this context, it is also tempting to hypothesize that, as shown in other systems, neuronal activity via intracellular calcium signals could trigger apoptosis, as reported during excitotoxicity (*Blanquie et al., 2017a*). The timing of SE-CRs death, namely the second postnatal week, corresponds to a major switch in cortical activity (*Luhmann and Khazipov, 2018*) and in GABAergic circuits (*Cossart, 2011*), raising the possibility that the elimination of CRs is part of a more global activity-dependent remodeling of cortical circuits. Irrespective of the underlying mechanism, surviving Kir2.1-expressing CRs displayed a relatively normal morphology, expressed Reln and received GABAergic synaptic inputs. Remarkably, SE-CRs is also the subpopulation undergoing a Bax-dependent apoptosis. Quantification of CRs that persist in both models suggests that a vast majority of SE-CRs survives. Indeed, in both deletion of *Bax* (*Ledonne et al., 2016*) or over-expression of Kir2.1 (this manuscript) models, a five-fold increase in CR numbers, corresponding to approximately 30% of the initial pool at P7, is detected when using the ΔNp73[Cre] line, in contrast to none when using the hem-specific Wnt3a[Cre] line. Since hem-CRs constitute about 70% of the population targeted by the ΔNp73[Cre] line (*Bielle et al., 2005*; *Yoshida et al., 2006*; *Tissir et al., 2009*), our findings support that the 30% of rescued CRs in ΔNp73[Cre] corresponds to a large fraction, if not all, of the SE-CR population. Together, these results demonstrate that hem-derived CRs die in a *Bax-* and activity-independent

manner, in contrast to SE-CRs that survive in Bax and Kir2.1 mutants. Hence, our work reveals that subpopulations of CRs are eliminated by very distinct mechanisms. Interestingly, hippocampal CRs, which mostly derive from the cortical hem (*Louvi et al., 2007*) display a delayed death which seems to occur independently of the apoptotic-specific Caspase-3 activity (*Anstötz et al., 2016*; *Anstötz et al., 2018*). Together, these data support the notion that CR subtypes are intrinsically different in the mechanism determining their demise and argues in favor of complex yet unappreciated subtype-specific pathways leading ultimately to cell death.

CRs aberrant survival perturbs the morphology and connectivity of upper layer neurons in an activity-dependent manner

In this work, we have demonstrated that SE-CRs persistence in mice has a strong effect on LII/III pyramidal neuron morphology and excitatory circuits. Notably, in the $\Delta Np73^{cre/+}$;Bax$^{lox/lox}$ mutants, we observed an impact on both apical and basal dendrites. While the effect on apical dendrites could be direct via local surviving SE-CRs, the impact on basal ones might be circuit-mediated since excitatory entries in apical dendritic tufts were shown to modify basal dendrite synaptic plasticity (*Williams and Holtmaat, 2019*). Moreover, SE-CRs survival leads in $\Delta Np73^{cre/+}$;Bax$^{lox/lox}$ mutants to increased synaptic density with major functional consequences on the E/I ratio. Conversely, recent work showed that aberrant reduction of CRs during development triggers decreased apical dendritic tufts and dendritic spine density of LII/III pyramidal neurons accompanied by a reduction in the E/I ratio (*de Frutos et al., 2016*). Taken together our findings reveal that the proper balance of CRs constitutes an essential, yet underappreciated, regulator of LII/III pyramidal neuron morphology and wiring.

Importantly, we found in both Bax and Kir models that surviving CRs are similarly kept embedded into functional networks. Interestingly, rescued CRs are also solely innervated by GABA$_A$ receptor-mediated synapses like their younger control counterparts. Although GABAergic synaptic connectivity often increases during postnatal development (*Pangratz-Fuehrer and Hestrin, 2011*), some cells may display transient connections that disappear after the second postnatal week, thereby accounting for the reduced connectivity observed in the two models. In contrast, since the effects on pyramidal neurons and cortical excitability are only found in *Bax* mutants, our study reveals that the inappropriate survival of SE-CRs drives an abnormal cortical wiring via an activity-dependent mechanism. However, CRs appear to act on upper layer pyramidal neurons *via* partially distinct mechanisms at different time points during development. Indeed, Kir2.1 expressing mice appear largely similar to controls, suggesting that the impact of reducing CR density on LII/III apical dendrites (*de Frutos et al., 2016*) does not rely exclusively on the intrinsic excitability of CRs. Nevertheless, the mechanism by which rescued CRs induce morphological and functional changes on pyramidal neurons remains unresolved. The lack of response observed during our optogenetic experiments suggest that these changes may not depend on a direct CR excitatory synaptic input onto principal neurons. This is in line with recent data obtained with experiments performed in the hippocampus using ChR2 activation and paired-recordings in the third postnatal week, where CRs are still present in high density (*Quattrocolo and Maccaferri, 2014*; *Anstötz et al., 2016*). Indeed, only very few pyramidal cells could be detected as an output of CR cells. Further experiments will be required to determine the relative roles of CR-secreted factors versus circuit-mediated effects onto apical and basal dendrites. Regardless the mechanism and since excitatory entries onto apical dendrites are emerging as major actors in sensory gating, cortical integration and reward (*Keller and Mrsic-Flogel, 2018*; *Khan and Hofer, 2018*; *Lacefield et al., 2019*; *Williams and Holtmaat, 2019*; *Zhang and Bruno, 2019*), our findings highlight the importance of a transient cell population in the emergence of functional circuits as well as the deleterious effects of their abnormal demise.

Our study thus shows that the elimination of SE-CRs in the somatosensory cortex is required for proper morphology and wiring of LII/III pyramidal neurons and reveals a remarkable interplay between activity, the elimination of transient cells and cortical wiring. Indeed, activity, likely driven by cortical maturation, regulates the elimination of transient CRs that would otherwise perturb upper layer wiring. Notably, CRs persistence has been described in human pathological conditions, often associated with epilepsy. Our work thus not only provides novel insights onto normal wiring of upper layers, but also addresses the functional consequences of incomplete CR removal with major relevance for neurodevelopmental diseases, such as autism spectrum disorder, schizophrenia or epilepsy.

Materials and methods

Key resources table

Reagent type (species) or resource	Designation	Source or reference	Identifiers	Additional information
Strain *Mus musculus* (males and female)	C57BL6J	Janvier		
Mus musculus (males and female)	ΔNp73^{CreIRESGFP}	*Tissir et al., 2009*	ΔNp73^{Cre}	
Mus musculus (males and female)	Wnt3a^{Cre}	*Yoshida et al., 2006*	Wnt3a^{Cre}	
Mus musculus (males and female)	Tau$^{loxP-stop-loxP-MARCKSeGFP-IRES-nlslacZ}$	*Hippenmeyer et al., 2005*	Tau^{GFP}	
Mus musculus (males and female)	Bax^{tm2Sjk}.Bak1^{tm1Thsn}/J	*Takeuchi et al., 2005*	Bax$^{lox/lox}$	
Mus musculus (males and female)	ROSA26$^{loxP-stop-loxP-Tomato}$	*Madisen et al., 2010*	R26^{mT}	
Mus musculus (males and female)	ROSA26$^{loxP-stop-loxP-Kcnj2-cherry/+}$	*Moreno-Juan et al., 2017*	R26$^{Kir2.1/+}$	
Mus musculus (males and female)	Ai32(RCL-ChR2 (H134R)/EYFP	https://www.jax.org/strain/012569	ChR2^{lox}	
Antibody	rabbit polyclonal anti-DsRed	Takara	RRID:AB_10013483	IF(1:500)
Antibody	mouse monoclonal anti-Reelin	Merck Millipore	RRID:AB_565117	IF(1:300)
Antibody	mouse monoclonal anti-Gephyrin	Synaptic systems	RRID:AB_2619837	IF(1:250)
Antibody	rabbit polyclonal anti-GAD65/67	Merck	RRID: AB_2278725	IF(1:250)
Antibody	guinea-pig anti-KCC2	D Ng and S Morton TM Jessell's lab		IF(1:4000)
Antibody	donkey anti-mouse Alexa-488	Jackson Immuno Research Laboratories	RRID:AB_2340846	IF(1:800)
Antibody	donkey anti-rabbit Cy3	Jackson ImmunoResearch Laboratories	RRID:AB_2307443	IF(1:800)
Antibody	donkey anti-rabbit Alexa-647	Molecular Probes	RRID:AB_2536183	IF(1:500)
Antibody	donkey anti-chick Alexa-488	Jackson ImmunoResearch Laboratories	RRID:AB_2340375	IF(1:1000)
Antibody	donkey anti-mouse Alexa-555	Molecular Probes	RRID:AB_2536180	IF(1:1000)
Antibody	goat anti-guinea pig Alexa-555	Molecular Probes	RRID:AB_2535856	IF(1:1000)
Antibody	DAPI (4', 6-diamidino-2-phenylindole)	Invitrogen Molecular Probes	RRID:AB_2629482	IF(1:2000)
Antibody	DyLight 488 streptavidin	Vector Labs	SP-4488	
Sequence-based reagent	CRE genotyping 188 f 167 r	This paper	PCR primers	188 f: TGA TGG ACA TGT TCA GGG ATC 167 r: GAA ATC AGT GCG TTC GAA CGC TAG A

Continued on next page

Continued

Reagent type (species) or resource	Designation	Source or reference	Identifiers	Additional information
Sequence-based reagent	$R26^{Kir2.1/+}$ genotyping AAY101 AAY103 SD297		PCR primers	AAY101: AAAGTCGCTCTGAGTTGTTAT (Rosa26 forward WT) AAY103: GGGAGCGGGAGAAATGGATATG (Rosa26 reverse WT) SD297: GGCCATTTACCGTAAGTTATG (CAG promoter reverse)
Chemical compound, drug	Paraformaldehyde	Sigma-Aldrich	CAT:P6148	
Chemical compound, drug	Triton 100X	Eurobio	CAT:GAUTTR00-07	
Chemical compound, drug	SR95531	Abcam	Ab120042	
Chemical compound, drug	4-AP	Sigma Aldrich	A-0152	
Software, algorithm	IMARIS software 8.4.	IMARIS	RRID:SCR_007370	
Software, algorithm	GraphPad Prism 7.0	GraphPad Software	RRID:SCR_000306	
Software, algorithm	ImageJ/FIJI	NIH	RRID:SCR_002285	
Software, algorithm	Adobe Photoshop CS6	Adobe Systems	RRID:SCR_014199	
Software, algorithm	pClamp10.1	Molecular Devices	RRID:SCR_011323	
Software, algorithm	IGOR Pro 6.0	Wavemetrics	RRID:SCR_000325	
Software, algorithm	NeuroMatic	Wavemetrics	RRID:SCR_004186	

Animals

$\Delta Np73^{CreIRESGFP}$($\Delta Np73^{Cre}$) (*Tissir et al., 2009*), $Wnt3a^{Cre}$ (*Yoshida et al., 2006*), $ROSA26^{loxP-stop-loxP-Tomato}$($R26^{mT}$) (*Madisen et al., 2010*), $Tau^{loxP-stop-loxP-MARCKSeGFP-IRES-nlslacZ}$ (Tau^{GFP}) (*Hippenmeyer et al., 2005*) and $ChR2^{lox}$ (Ai32(RCL-ChR2(H134R)/EYFP) (https://www.jax.org/strain/012569)) transgenic mice were kept in a C57BL/6J background. The Bax^{tm2Sjk};$Bak1^{tm1Thsn}$/J line (*Takeuchi et al., 2005*) harboring the floxed *Bax* and the *Bak* knock-out alleles was purchased from the Jackson laboratory as mixed B6;129. $\Delta Np73^{Cre}$ and $Wnt3a^{Cre}$ lines were crossed with the $R26^{mT}$ or Tau^{GFP} reporter lines to permanently label CR subtypes. $\Delta Np73^{Cre}$ line was crossed to the Bax^{tm2Sjk};$Bak1^{tm1Thsn}$/J line ($Bax^{lox/lox}$) to inactivate Bax function in specific CR subtypes. The conditional knock-out also harbored a reporter allele $R26^{mT}$ in order to trace the neurons in which recombination had occurred. $\Delta Np73^{Cre}$ and $Wnt3a^{Cre}$ lines were crossed to $ROSA26^{loxP-stop-loxP-Kcnj2-cherry/+}$ ($R26^{Kir2.1/+}$) (*Moreno-Juan et al., 2017*) to overexpress the *Kcnj2* gene, which encodes Kir2.1, in specific CR subpopulations. Controls used were littermates heterozygous *Bax* for the Bax model and $\Delta Np73^{+/+}$;$R26^{Kir2.1/+}$ for the Kir2.1 model. Animals were genotyped by PCR using primers specific for the different alleles. All animals were handled in strict accordance with good animal practice as defined by the national animal welfare bodies, and all mouse work was approved by the Veterinary Services of Paris (Authorization number: 75–1454) and by the Animal Experimentation Ethical Committee Buffon (CEEA-40) (Reference: CEB-34–2012) and by the Animal Experimentation Ethical Committee Darwin (Reference: 02224.02).

Tissue preparation and immunohistochemistry

For staging of animals, the birth date was considered as postnatal day 0 (P0). Animals were anesthetized with Isoflurane and intracardially perfused with 4% paraformaldehyde (PFA) in 0.1 M PBS, pH 7.4 and post-fixed over-night in 4% PFA at 4°C. Brain were embedded in 3.5% agarose and sectioned in 70 µm free-floating slices at all stages in *Figure 1* and *Figure 1—figure supplement 1*. For

Figure 2—figure supplement 1E, brains were cryoprotected and sectioned in 50 µm free-floating slices. Immunostaining was performed as previously described (*Bielle et al., 2005*; *Griveau et al., 2010*; *de Frutos et al., 2016*). Primary antibodies used for immunohistochemistry were: mouse anti-Reelin (MAB5364, Millipore 1:300), rabbit anti-DsRed (Takara 632496, 1:500), mouse anti-Gephyrin (147 011, Synaptic Systems, 1:250), Rabbit anti-GAD65/67 (AB1511, Merck, 1:250), guinea pig anti-KCC2 (Gift of S.Morton and D.Ng, 1:4000). Secondary antibodies used against primary antibodies were: donkey anti-mouse Alexa-488 (Jackson ImmunoResearch Laboratories, 1:800), donkey anti-rabbit Cy3 (Jackson ImmunoResearch Laboratories, 1:800), donkey anti-chick Alexa-488 (Jackson ImmunoResearch Laboratories, 1:1000), donkey anti-mouse Alexa-555 (A-31570, Molecular Probes, 1:1000), donkey anti-rabbit Alexa-647 (A31573, Molecular Probes, 1:500), goat anti-guinea pig Alexa-555 (A-21435, Molecular Probes, 1:1000). Hoechst (Sigma-Aldrich 33342, 1:1000) and DAPI (D1306, ThermoFisher Scientific, 1:2000) were used for fluorescent nuclear counterstaining the tissue and mounting was done in Vectashield (Vector Labs).

Image acquisition and cell countings

Immunofluorescence images were acquired using a confocal microscope (Leica TCS SP5), except for anti-KCC2, Gephyrin and GAD65/67 (*Figure 2—figure supplement 1E, f*) that were acquired on a LEICA SP8 confocal microscope with 93X objective and 2.5 digital zoom (a single optical plane or around 100 z-stacks of 0.07 µm respectively). DsRed$^+$ neurons, detected by immunofluorescence, were counted using the ImageJ software, in the somatosensory barrel cortex (S1) for each age and genotype. For each section, the density of CRs (DsRed$^+$ CRs/mm^3) was calculated taking into account the thickness of the section and the surface of Layer I, measured using ImageJ software.

Acute slice preparation, electrophysiology and photostimulation

Acute coronal slices (300 µm) of the neocortex were obtained from $\Delta Np73^{cre/+};Bax^{lox/lox}$ and $\Delta Np73^{cre/+};R26^{Kir2.1/+}$ mutants. Excitation light to visualize the tdTomato or Cherry fluorescent proteins was provided by a green Optoled Light Source (Cairn Research, UK) and images were collected with an iXon+ 14-bit digital camera (Andor Technology, UK), as previously described (*Orduz et al., 2015*). Patch-clamp recordings were performed at RT using an extracellular solution containing (in mM): 126 NaCl, 2.5 KCl, 1.25 NaH$_2$PO$_4$, 26 NaHCO$_3$, 20 glucose, five pyruvate, 2 CaCl$_2$ and 1 MgCl$_2$ (95% O$_2$, 5% CO$_2$). Fluorescent CRs were recorded at P13-17 and P24-29 with different intracellular solutions according to the experiment and containing (in mM): either 130 K-Gluconate (K-Glu) or 130 KCl, 0.1 EGTA, 0.5 CaCl$_2$, 2 MgCl$_2$, 10 HEPES, 2 Na$_2$-ATP, 0.2 Na-GTP and 10 Na$_2$-phosphocreatine and 5.4 mM biocytin (pH $\approx$ 7.3). When using a KGlu-based intracellular solution in whole-cell configuration, potentials were corrected for a junction potential of -10 mV. Recordings were made without series resistance (R$_s$) compensation; R$_s$ was monitored during recordings and cells showing a change of more than 20% in R$_s$ were discarded. To evaluate the effect of SR95351 (10 µM; Abcam, Cambridge, UK), drug perfusion reached a steady state at 3 min in the recording chamber. This time was respected before quantification of either spontaneous or evoked PSCs. To test for the presence of eEPSCs mediated by NMDARs receptors at hyperpolarized potentials, the extracellular concentration of MgCl$_2$ was replaced by CaCl$_2$ in order to relieve the Mg^{2+} block of these receptors.

Photostimulation of fluorescent ChR2-expressing rescued CRs recorded in whole-cell configuration was obtained by triggering light trains with a blue LED (470 nm, 1 ms pulses; Optoled Light Source, Cairn Research, UK). Light trains of 2, 5, 10 and 20 Hz during 10 s or 30 s were applied to define the optimal frequency inducing an effective activation of recorded ChR2-expressing rescued CRs. For each frequency, we calculated the number of spikes (Ns) with respect to the number of light pulses (NLP) and determined the percentage of success as [Ns/NLP] x 100. To test the effect of rescued CRs activation, we performed extracellular recordings and patch-clamp recordings of Layer I interneurons while stimulating with light trains (5 Hz, 10 s or 30 s). Extracellular recordings were recorded with a patch pipette filled with extracellular solution. In a set of experiments, the extracellular solution contained 0 mM Mg^{2+}, 3 mM Ca^{2+} and 4AP for more than 5 min at least.

Recordings were obtained using Multiclamp 700B and pClamp10.1 (Molecular Devices), filtered at 4 kHz and digitized at 20 kHz. Digitized data were analyzed off-line using Neuromatic within IGOR Pro 6.0 environment (Wavemetrics, USA) (*Rothman and Silver, 2018*). Extracellular

stimulations were performed using a monopolar electrode (glass pipette) placed in Layer I for CRs and Layer II/III for pyramidal neurons (20–99 V, 100 µs stimulations each 8–12 s; Iso-Stim 01D, npi electronic GmbH, Tamm, Germany). Spontaneous postsynaptic currents were detected with a threshold of 2 times the noise standard deviation during a time window of 3 min for CRs and 1.5 min for pyramidal cells. The Vm was estimated in current-clamp mode as soon as the whole-cell configuration was established. The analysis of Rin, action potential amplitudes and duration was performed during pulses of 800 ms in current-clamp configuration from −80 mV during increasing steps of 5 pA as previously described (*Ledonne et al., 2016*).

Morphological analyses

For morphological analysis, CRs and layer II/III pyramidal cells were loaded with biocytin through patch pipette during whole-cell recordings. The slices were fixed 2 hr in 4% paraformaldehyde at 4° C, rinsed three times in PBS for 10 min, and incubated with 1% triton X-100% and 2% BSA during 1 hr. Then, they were washed three times in PBS and incubated in DyLight 488 streptavidin (Vector Labs, Burlingame, USA) for 2 hr. Successfully labeled CRs and Layer II/III pyramidal cells were visualized either using a LEICA SP5 or SP8 confocal microscope with a 40X objective and a 1.3 digital zoom. Around 250 optical sections of 0.6 µm were necessary to image the whole dendritic tree of each neuron. For dendritic spines, images of apical dendrites in Layer I and basal dendrites in Layer II/III were acquired with a 63X objective (100 optical sections of 0.25 µm each). For apical dendrites, a terminal ramification in Layer I was acquired, while for basal dendrites a horizontal dendrite in Layer II/III was acquired approximately at 60 µm distance from the soma after the first ramification. 3D reconstruction was performed using the IMARIS software 8.4. Statistical analyses were performed based on the data given by IMARIS in apical and basal dendrites separately. Counting of spines was performed manually using ImageJ software on black and white maximum projections on two different segments approximately 50 µm long for each image. For morphological analysis of CRs, statistical analyses were performed based on the values calculated by image analyses using the IMARIS software (soma diameter and filament length).

Statistical analysis

All data were expressed as mean ± SEM. A P-value less than 0.05 was considered significant. For statistical groups larger than 7, we performed a D'Agostino-Pearson normality test. According to the data structure, two-group comparisons were performed using two-tailed unpaired Student T test or Mann-Whitney U Test. Bonferroni multiple comparisons were used as post-hoc test following one-way or two-way ANOVA or the non-parametric Kruskal-Wallis Tests. For small statistical groups (less than 7), we systematically performed non-parametric tests (Mann-Whitney U Test or Kruskal-Wallis Tests with Dunn's correction). A reconstructed pyramidal neuron displaying an exceptional basal dendrite projecting to Layer I was submitted to Grubbs test and excluded as an extreme outlier. Statistics and plotting were performed using GraphPad Prism 7.00 (GraphPad Software Inc, USA). *p<0.05, **p<0.01, ***p<0.001.

Additional information

Funding

Funder	Grant reference number	Author
Agence Nationale de la Recherche	ANR-15-CE16-0003-01	Alessandra Pierani Maria Cecilia Angulo Sonia Garel
Fondation pour la Recherche Médicale	Equipe (DEQ20130326521)	Alessandra Pierani
Fondation pour la Recherche Médicale	Equipe (DEQ20150331681)	Maria Cecilia Angulo
European Commission	ERC-2013-CoG-616080	Sonia Garel
Ministry of Higher Education, Research and Innovation	Fellowship	Martina Riva Ioana Genescu
Ministry of Science, Innovation and Universities	BFU2015-64432-R	Guillermina López-Bendito
European Commission	ERC-2014-CoG-647012	Guillermina López-Bendito
Fondation pour l'Aide à la Recherche sur la Sclérose en Plaques	Postdoctoral fellowship	Chloé Habermacher

The funders had no role in study design, data collection and interpretation, or the decision to submit the work for publication.

Author contributions

Martina Riva, Ioana Genescu, Chloé Habermacher, David Orduz, Eva Coppola, Conceptualization, Data curation, Formal analysis, Validation, Visualization, Methodology, Writing—original draft, Writing—review and editing; Fanny Ledonne, Data curation, Formal analysis, Supervision, Validation, Visualization, Methodology; Filippo M Rijli, Guillermina López-Bendito, Resources; Sonia Garel, Alessandra Pierani, Conceptualization, Resources, Formal analysis, Supervision, Funding acquisition, Validation, Investigation, Visualization, Methodology, Writing—original draft, Project administration, Writing—review and editing; Maria Cecilia Angulo, Conceptualization, Formal analysis, Supervision, Funding acquisition, Validation, Investigation, Visualization, Methodology, Writing—original draft, Project administration, Writing—review and editing

Author ORCIDs

David Orduz https://orcid.org/0000-0002-4198-2691
Filippo M Rijli http://orcid.org/0000-0003-0515-0182
Sonia Garel https://orcid.org/0000-0003-2984-3645
Maria Cecilia Angulo https://orcid.org/0000-0002-0758-0496
Alessandra Pierani https://orcid.org/0000-0002-4872-4791

Ethics

Animal experimentation: All animals were handled in strict accordance with good animal practice as defined by the national animal welfare bodies, and all mouse work was approved by the Veterinary Services of Paris (Authorization number: 75-1454) and by the Animal Experimentation Ethical

Committee Buffon (CEEA-40) (Reference: CEB-34-2012) and by the Animal Experimentation Ethical Committee Darwin (Reference: 02224.02).

Decision letter and Author response

Decision letter https://doi.org/10.7554/eLife.50503.sa1
Author response https://doi.org/10.7554/eLife.50503.sa2

Additional files

Supplementary files
• Transparent reporting form

Data availability
All data generated or analysed during this study are included in the manuscript and supporting files. The Source data file contains all the data presented in the figures (1 sheet per Figure).

References

Achilles K, Okabe A, Ikeda M, Shimizu-Okabe C, Yamada J, Fukuda A, Luhmann HJ, Kilb W. 2007. Kinetic properties of cl uptake mediated by na+-dependent K+-2Cl cotransport in immature rat neocortical neurons. *Journal of Neuroscience* **27**:8616–8627. DOI: https://doi.org/10.1523/JNEUROSCI.5041-06.2007, PMID: 176 87039

Anstötz M, Cosgrove KE, Hack I, Mugnaini E, Maccaferri G, Lübke JH. 2014. Morphology, input-output relations and synaptic connectivity of Cajal-Retzius cells in layer 1 of the developing neocortex of CXCR4-EGFP mice. *Brain Structure and Function* **219**:2119–2139. DOI: https://doi.org/10.1007/s00429-013-0627-2, PMID: 240262 87

Anstötz M, Huang H, Marchionni I, Haumann I, Maccaferri G, Lübke JH. 2016. Developmental profile, morphology, and synaptic connectivity of Cajal-Retzius cells in the postnatal mouse Hippocampus. *Cerebral Cortex* **26**:855–872. DOI: https://doi.org/10.1093/cercor/bhv271, PMID: 26582498

Anstötz M, Lee SK, Neblett TI, Rune GM, Maccaferri G. 2018. Experience-Dependent regulation of Cajal-Retzius cell networks in the developing and adult mouse Hippocampus. *Cerebral Cortex* **28**:672–687. DOI: https://doi. org/10.1093/cercor/bhx153, PMID: 28637318

Barber M, Arai Y, Morishita Y, Vigier L, Causeret F, Borello U, Ledonne F, Coppola E, Contremoulins V, Pfrieger FW, Tissir F, Govindan S, Jabaudon D, Proux-Gillardeaux V, Galli T, Pierani A. 2015. Migration speed of Cajal-Retzius cells modulated by vesicular trafficking controls the size of Higher-Order cortical Areas. *Current Biology* **25**:2466–2478. DOI: https://doi.org/10.1016/j.cub.2015.08.028, PMID: 26387718

Barber M, Pierani A. 2016. Tangential migration of glutamatergic neurons and cortical patterning during development: lessons from Cajal-Retzius cells. *Developmental Neurobiology* **76**:847–881. DOI: https://doi.org/ 10.1002/dneu.22363

Bielle F, Griveau A, Narboux-Nême N, Vigneau S, Sigrist M, Arber S, Wassef M, Pierani A. 2005. Multiple origins of Cajal-Retzius cells at the borders of the developing pallium. *Nature Neuroscience* **8**:1002–1012. DOI: https:// doi.org/10.1038/nn1511, PMID: 16041369

Blanquie O, Kilb W, Sinning A, Luhmann HJ. 2017a. Homeostatic interplay between electrical activity and neuronal apoptosis in the developing neocortex. *Neuroscience* **358**:190–200. DOI: https://doi.org/10.1016/j. neuroscience.2017.06.030, PMID: 28663094

Blanquie O, Liebmann L, Hübner CA, Luhmann HJ, Sinning A. 2017b. NKCC1-Mediated GABAergic signaling promotes postnatal cell death in neocortical Cajal-Retzius cells. *Cerebral Cortex* **27**:1644–1659. DOI: https:// doi.org/10.1093/cercor/bhw004, PMID: 26819276

Causeret F, Coppola E, Pierani A. 2018. Cortical developmental death: selected to survive or fated to die. *Current Opinion in Neurobiology* **53**:35–42. DOI: https://doi.org/10.1016/j.conb.2018.04.022, PMID: 29738999

Chen J, Kriegstein AR. 2015. A GABAergic projection from the zona incerta to cortex promotes cortical neuron development. *Science* **350**:554–558. DOI: https://doi.org/10.1126/science.aac6472, PMID: 26429884

Cocas LA, Fernandez G, Barch M, Doll J, Zamora Diaz I, Pleasure SJ. 2016. Cell Type-Specific circuit mapping reveals the presynaptic connectivity of developing cortical circuits. *Journal of Neuroscience* **36**:3378–3390. DOI: https://doi.org/10.1523/JNEUROSCI.0375-15.2016, PMID: 26985044

Cossart R. 2011. The maturation of cortical interneuron diversity: how multiple developmental journeys shape the emergence of proper network function. *Current Opinion in Neurobiology* **21**:160–168. DOI: https://doi. org/10.1016/j.conb.2010.10.003, PMID: 21074988

de Frutos CA, Bouvier G, Arai Y, Thion MS, Lokmane L, Keita M, Garcia-Dominguez M, Charnay P, Hirata T, Riethmacher D, Grove EA, Tissir F, Casado M, Pierani A, Garel S. 2016. Reallocation of olfactory Cajal-Retzius cells shapes neocortex architecture. *Neuron* **92**:435–448. DOI: https://doi.org/10.1016/j.neuron.2016.09.020, PMID: 27693257

Del Río JA, Heimrich B, Supèr H, Borrell Víctor, Frotscher M, Soriano E. 1996. Differential survival of Cajal–Retzius Cells in Organotypic Cultures of Hippocampus and Neocortex. *The Journal of Neuroscience* **16**:6896–6907. DOI: https://doi.org/10.1523/JNEUROSCI.16-21-06896.1996

Fuchs Y, Steller H. 2011. Programmed cell death in animal development and disease. *Cell* **147**:742–758. DOI: https://doi.org/10.1016/j.cell.2011.10.033, PMID: 22078876

Griveau A, Borello U, Causeret F, Tissir F, Boggetto N, Karaz S, Pierani A. 2010. A novel role for Dbx1-derived Cajal-Retzius cells in early regionalization of the cerebral cortical neuroepithelium. *PLOS Biology* **8**:e1000440. DOI: https://doi.org/10.1371/journal.pbio.1000440, PMID: 20668538

Hippenmeyer S, Vrieseling E, Sigrist M, Portmann T, Laengle C, Ladle DR, Arber S. 2005. A developmental switch in the response of DRG neurons to ETS transcription factor signaling. *PLOS Biology* **3**:e159. DOI: https://doi.org/10.1371/journal.pbio.0030159, PMID: 15836427

Ishii K, Kubo KI, Nakajima K. 2016. Reelin and neuropsychiatric disorders. *Frontiers in Cellular Neuroscience* **10**:229. DOI: https://doi.org/10.3389/fncel.2016.00229, PMID: 27803648

Keller GB, Mrsic-Flogel TD. 2018. Predictive processing: a canonical cortical computation. *Neuron* **100**:424–435. DOI: https://doi.org/10.1016/j.neuron.2018.10.003, PMID: 30359606

Khan AG, Hofer SB. 2018. Contextual signals in visual cortex. *Current Opinion in Neurobiology* **52**:131–138. DOI: https://doi.org/10.1016/j.conb.2018.05.003, PMID: 29883940

Kilb W, Luhmann HJ. 2001. Spontaneous GABAergic postsynaptic currents in Cajal-Retzius cells in neonatal rat cerebral cortex. *European Journal of Neuroscience* **13**:1387–1390. DOI: https://doi.org/10.1046/j.0953-816x.2001.01514.x, PMID: 11298799

Kirischuk S, Luhmann HJ, Kilb W. 2014. Cajal-Retzius cells: update on structural and functional properties of these mystic neurons that bridged the 20th century. *Neuroscience* **275**:33–46. DOI: https://doi.org/10.1016/j.neuroscience.2014.06.009, PMID: 24931764

Kirmse K, Dvorzhak A, Henneberger C, Grantyn R, Kirischuk S. 2007. Cajal retzius cells in the mouse neocortex receive two types of pre- and postsynaptically distinct GABAergic inputs. *The Journal of Physiology* **585**:881–895. DOI: https://doi.org/10.1113/jphysiol.2007.145003, PMID: 17962325

Kolbaev SN, Achilles K, Luhmann HJ, Kilb W. 2011. Effect of depolarizing GABA(A)-mediated membrane responses on excitability of Cajal-Retzius cells in the immature rat neocortex. *Journal of Neurophysiology* **106**:2034–2044. DOI: https://doi.org/10.1152/jn.00699.2010, PMID: 21775719

Lacefield CO, Pnevmatikakis EA, Paninski L, Bruno RM. 2019. Reinforcement learning recruits somata and apical dendrites across layers of primary sensory cortex. *Cell Reports* **26**:2000–2008. DOI: https://doi.org/10.1016/j.celrep.2019.01.093

Ledonne F, Orduz D, Mercier J, Vigier L, Grove EA, Tissir F, Angulo MC, Pierani A, Coppola E. 2016. Targeted inactivation of bax reveals a Subtype-Specific mechanism of Cajal-Retzius neuron death in the postnatal cerebral cortex. *Cell Reports* **17**:3133–3141. DOI: https://doi.org/10.1016/j.celrep.2016.11.074, PMID: 28009284

Louvi A, Yoshida M, Grove EA. 2007. The derivatives of the Wnt3a lineage in the central nervous system. *The Journal of Comparative Neurology* **504**:550–569. DOI: https://doi.org/10.1002/cne.21461, PMID: 17701978

Luhmann HJ. 2013. Cajal-Retzius and Subplate cells: Transient Cortical neurons and Circuits. In: Rubenstein J. L. R, Rakic P (Eds). *Cellular Migration and Formation of Neuronal Connections: Comprehensive Developmental Neuroscience.* Academic Press. p. 843–856. DOI: https://doi.org/10.1016/B978-0-12-397266-8.00009-0

Luhmann HJ, Khazipov R. 2018. Neuronal activity patterns in the developing barrel cortex. *Neuroscience* **368**:256–267. DOI: https://doi.org/10.1016/j.neuroscience.2017.05.025, PMID: 28528963

Madisen L, Zwingman TA, Sunkin SM, Oh SW, Zariwala HA, Gu H, Ng LL, Palmiter RD, Hawrylycz MJ, Jones AR, Lein ES, Zeng H. 2010. A robust and high-throughput cre reporting and characterization system for the whole mouse brain. *Nature Neuroscience* **13**:133–140. DOI: https://doi.org/10.1038/nn.2467, PMID: 20023653

Mienville JM. 1998. Persistent depolarizing action of GABA in rat Cajal-Retzius cells. *The Journal of Physiology* **512**:809–817. DOI: https://doi.org/10.1111/j.1469-7793.1998.809bd.x, PMID: 9769423

Mienville JM, Pesold C. 1999. Low resting potential and postnatal upregulation of NMDA receptors may cause Cajal-Retzius cell death. *The Journal of Neuroscience* **19**:1636–1646. DOI: https://doi.org/10.1523/JNEUROSCI.19-05-01636.1999, PMID: 10024350

Moreno-Juan V, Filipchuk A, Antón-Bolaños N, Mezzera C, Gezelius H, Andrés B, Rodríguez-Malmierca L, Susín R, Schaad O, Iwasato T, Schüle R, Rutlin M, Nelson S, Ducret S, Valdeolmillos M, Rijli FM, López-Bendito G. 2017. Prenatal thalamic waves regulate cortical area size prior to sensory processing. *Nature Communications* **8**:14172. DOI: https://doi.org/10.1038/ncomms14172, PMID: 28155854

Myakhar O, Unichenko P, Kirischuk S. 2011. GABAergic projections from the subplate to Cajal-Retzius cells in the neocortex. *NeuroReport* **22**:525–529. DOI: https://doi.org/10.1097/WNR.0b013e32834888a4, PMID: 21666518

Orduz D, Maldonado PP, Balia M, Vélez-Fort M, de Sars V, Yanagawa Y, Emiliani V, Angulo MC. 2015. Interneurons and oligodendrocyte progenitors form a structured synaptic network in the developing neocortex. *eLife* **4**:e06953. DOI: https://doi.org/10.7554/eLife.06953

Pangratz-Fuehrer S, Hestrin S. 2011. Synaptogenesis of electrical and GABAergic synapses of fast-spiking inhibitory neurons in the neocortex. *Journal of Neuroscience* **31**:10767–10775. DOI: https://doi.org/10.1523/JNEUROSCI.6655-10.2011, PMID: 21795529

Pozas E, Paco S, Soriano E, Aguado F. 2008. Cajal-Retzius cells fail to trigger the developmental expression of the cl- extruding co-transporter KCC2. *Brain Research* **1239**:85–91. DOI: https://doi.org/10.1016/j.brainres.2008.08.058, PMID: 18789906

Quattrocolo G, Maccaferri G. 2014. Optogenetic activation of cajal-retzius cells reveals their glutamatergic output and a novel feedforward circuit in the developing mouse Hippocampus. *Journal of Neuroscience* **34**: 13018–13032. DOI: https://doi.org/10.1523/JNEUROSCI.1407-14.2014, PMID: 25253849

Radnikow G, Feldmeyer D, Lübke J. 2002. Axonal projection, input and output synapses, and synaptic physiology of Cajal–Retzius Cells in the Developing Rat Neocortex. *The Journal of Neuroscience* **22**:6908–6919. DOI: https://doi.org/10.1523/JNEUROSCI.22-16-06908.2002

Rothman JS, Silver RA. 2018. NeuroMatic: an integrated Open-Source software toolkit for acquisition, analysis and simulation of electrophysiological data. *Frontiers in Neuroinformatics* **12**:14. DOI: https://doi.org/10.3389/fninf.2018.00014, PMID: 29670519

Sava BA, Dávid CS, Teissier A, Pierani A, Staiger JF, Luhmann HJ, Kilb W. 2010. Electrophysiological and morphological properties of Cajal–Retzius cells with different ontogenetic origins. *Neuroscience* **167**:724–734. DOI: https://doi.org/10.1016/j.neuroscience.2010.02.043

Schwartz TH, Rabinowitz D, Unni V, Kumar VS, Smetters DK, Tsiola A, Yuste R. 1998. Networks of coactive neurons in developing layer 1. *Neuron* **20**:541–552. DOI: https://doi.org/10.1016/S0896-6273(00)80993-9

Soda T, Nakashima R, Watanabe D, Nakajima K, Pastan I, Nakanishi S. 2003. Segregation and coactivation of developing neocortical layer 1 neurons. *The Journal of Neuroscience* **23**:6272–6279. DOI: https://doi.org/10.1523/JNEUROSCI.23-15-06272.2003, PMID: 12867512

Sun L, Chen R, Bai Y, Li J, Wu Q, Shen Q, Wang X. 2019. Morphological and physiological characteristics of Ebf2-EGFP-Expressing Cajal-Retzius cells in developing mouse neocortex. *Cerebral Cortex* **29**:3864–3878. DOI: https://doi.org/10.1093/cercor/bhy265, PMID: 30307495

Takeuchi O, Fisher J, Suh H, Harada H, Malynn BA, Korsmeyer SJ. 2005. Essential role of BAX,BAK in B cell homeostasis and prevention of autoimmune disease. *PNAS* **102**:11272–11277. DOI: https://doi.org/10.1073/pnas.0504783102

Tissir F, Ravni A, Achouri Y, Riethmacher D, Meyer G, Goffinet AM. 2009. DeltaNp73 regulates neuronal survival in vivo. *PNAS* **106**:16871–16876. DOI: https://doi.org/10.1073/pnas.0903191106, PMID: 19805388

Williams LE, Holtmaat A. 2019. Higher-Order thalamocortical inputs gate synaptic Long-Term potentiation via disinhibition. *Neuron* **101**:91–102. DOI: https://doi.org/10.1016/j.neuron.2018.10.049

Wong FK, Marín O. 2019. Developmental cell death in the cerebral cortex. *Annual Review of Cell and Developmental Biology* **35**:523–542. DOI: https://doi.org/10.1146/annurev-cellbio-100818-125204, PMID: 31283379

Yoshida M, Assimacopoulos S, Jones KR, Grove EA. 2006. Massive loss of Cajal-Retzius cells does not disrupt neocortical layer order. *Development* **133**:537–545. DOI: https://doi.org/10.1242/dev.02209, PMID: 16410414

Zhang W, Bruno RM. 2019. High-order thalamic inputs to primary somatosensory cortex are stronger and longer lasting than cortical inputs. *eLife* **8**:e44158. DOI: https://doi.org/10.7554/eLife.44158, PMID: 30741160